Available online at www.sciencedirect.com
ScienceDirect
Journal of Computational Physics 221 (2007) 600–614
JOURNAL OF COMPUTATIONAL PHYSICS
www.elsevier.com/locate/jcp

A ghost-fluid method for large-eddy simulations of premixed combustion in complex geometries

V. Moureau [a,*], P. Minot [a], H. Pitsch [a], C. Bérat [b]

[a] CTR, Stanford University, Building 500, Stanford, CA 94305, USA
[b] Turboméca – Safran Group, 64522 Bordes, France

Received 13 March 2006; received in revised form 3 June 2006; accepted 21 June 2006
Available online 14 August 2006

Abstract

In this paper, a new ghost-fluid method for interfaces of finite thickness is described. It allows to compute efficiently turbulent premixed flames with a finite thickness in low-Mach flows. A level set algorithm is used to track accurately the flame and to define the overlapping region where the burned and unburned gases satisfy the jump conditions. These algorithms are combined with a fractional-step method to alleviate the acoustic CFL constraint. The full algorithm is verified for simple flame–vortex interactions and it is validated by computing a turbulent flame anchored by a triangular flame-holder. Finally, the algorithm is applied in the LES of an industrial lean-premixed swirl-burner.

Keywords: LES; Ghost-fluid method; Premixed combustion; Fractional-step method

1. Motivation and objectives

Large-eddy simulation of premixed combustion is a computational challenge, because complex diffusion and reaction processes often occur in very thin layers. The interaction of these processes with turbulence determines the main properties of the flame brush, such as its burning velocity or its thickness. In turbulent flows, the large vortices wrinkle the flame brush and increase the flame surface, while the small scales may penetrate into the flame and increase the flame thickness. In both cases, the turbulence leads to an increase in the burning velocity. This feature has to be captured by a combustion model. Even if the turbulent scales increase the flame thickness, the flame brush remains difficult to resolve on LES meshes. Numerically, the premixed flame brush is very close to an interface, but its non-zero thickness must be taken into account to represent the flame–turbulence interactions properly.

In state-of-the-art combustion models, the issue of thin flames is overcome in very different ways. The thickened-flame model (TFLES) [1] artificially thickens the flame brush, and the source terms in the species and energy equations are corrected to recover the correct burning velocity. The thickening factor to resolve the flame on a usual unstructured mesh is on the order of 20. This factor can be decreased slightly if naturally

* Corresponding author.
E-mail addresses: vincent.moureau@centraliens.net, moureauv@stanford.edu (V. Moureau).

0021-9991/$ - see front matter
doi:10.1016/j.jcp.2006.06.031

thicker quantities are used to represent the flame. This is the case in flame surface density approaches [2], but the thickening factor remains large. Instead of transporting reacting scalars, the flame can also be described using a flamelet hypothesis. That is, the reaction zone in the flame is considered to retain a laminar structure. The problem is then reduced to finding the position of the thin reaction layer. This is the principle of the *G*-equation model [3,4] in which a level set technique is used to track accurately the flame front. The displacement velocity of the level set is usually given by a model based on asymptotic analysis or experimental correlations [4,5]. Then, the level set has to be coupled with the Navier–Stokes solver by imposing the temperature profile in the flame brush. Often, Navier–Stokes solvers are not able to deal with large density and momentum gradients, and the imposed temperature profile has to be resolved on more than one cell, typically on the order of five cells.

In all the described models, the flame brush is more or less thickened, and the interactions with the smallest resolved scales are modified. The proposed method overcomes this artificial thickening using a numerical method that better couples the level set technique and the Navier–Stokes solver. This method is based on the ghost-fluid method (GFM) [6], which tracks discontinuities without introducing any smearing or numerical instabilities. While the original GFM has been developed to track infinitely thin discontinuities, the present method extends the GFM formalism to deal with interfaces of finite thickness.

2. A ghost-fluid method for thin flame brushes

2.1. The classical variable-density method for low-Mach number flows

In reacting flows, the density is not constant, and incompressible methods cannot be used. Taking the low-Mach limit without the constant-density assumption, the filtered Navier–Stokes equations reduce to the continuity and momentum equations:

$$\frac{\partial \bar{\rho}}{\partial t} + \nabla \cdot (\bar{\rho}\tilde{\mathbf{u}}) = 0, \tag{1}$$

$$\frac{\partial \bar{\rho}\tilde{\mathbf{u}}}{\partial t} + \nabla \cdot (\bar{\rho}\tilde{\mathbf{u}}\tilde{\mathbf{u}}) = -\nabla \overline{P} + \nabla \cdot \mathbf{t}, \tag{2}$$

where $\bar{}$ and $\tilde{}$ denote the LES filtering and the mass weighted filtering, respectively. ρ is the density, $\mathbf{u}$ is the velocity, P is the pressure and $\mathbf{t}$ is the total stress tensor. In (1) and (2), the density is usually given from the combustion model. The pressure in (2) is not the thermodynamic pressure but rather a Lagrange multiplier called dynamic pressure. Similar to incompressible flows, these equations can be solved using a fractional-step method. A time-staggered discretization of (1) is given as:

$$\frac{\bar{\rho}^{n+3/2} - \bar{\rho}^{n+1/2}}{\Delta t} + \nabla \cdot (\bar{\rho}\tilde{\mathbf{u}}^{n+1}) = 0. \tag{3}$$

If the density is known at $t^{n+1/2}$ and $t^{n+3/2}$, this equation provides a constraint on the velocity divergence. The first step of the fractional-step method is to advance the momentum equation to:

$$\frac{\bar{\rho}\tilde{\mathbf{u}}^{\star} - \bar{\rho}\tilde{\mathbf{u}}^{n}}{\Delta t} + \nabla \cdot (\bar{\rho}\tilde{\mathbf{u}}^{n+1/2}\tilde{\mathbf{u}}^{n+1/2}) = \nabla \cdot \mathbf{t}. \tag{4}$$

In the second step, the momentum is corrected with the dynamic pressure gradient:

$$\frac{\bar{\rho}\tilde{\mathbf{u}}^{n+1} - \bar{\rho}\tilde{\mathbf{u}}^{\star}}{\Delta t} = -\nabla \overline{P}^{n+1/2}. \tag{5}$$

The dynamic pressure $\overline{P}$ is found solving the variable-density Poisson equation:

$$\nabla \cdot \nabla \overline{P}^{n+1/2} = \frac{\bar{\rho}^{n+3/2} - \bar{\rho}^{n+1/2}}{\Delta t^2} + \frac{1}{\Delta t}\nabla \cdot (\bar{\rho}\tilde{\mathbf{u}}^{\star}). \tag{6}$$

Solving (4)–(6) for a propagating premixed flame may present several challenges. First, since the flame essentially occurs on the sub-filter scale, the filtered velocity and momentum flux may have steep gradients, which are difficult to integrate in the momentum equation. This may lead to spurious numerical instabilities. Second,

the density variations in the flame may also be large. These density variations have to be integrated in the RHS of the Poisson equation, which may lead to the generation of non-physical velocity waves immediately propagated throughout the whole computational domain.

2.2. The ghost-fluid method principle

The ghost-fluid method [6] applied to premixed combustion removes the steep gradients in the spatial derivatives by solving two continuous problems in the unburned and burned gases, and by satisfying jump conditions at the interface, as shown in Fig. 1. To impose the jump conditions, the two continuous problems have to be solved in an overlapping region around the flame brush. The level set formalism is well adapted to track the flame position and to define the regions where each problem has to be solved.

The main idea of the present method is to advance the momentum in the unburned and burned gases independently and then to use a modified Poisson equation to impose the jump conditions and the continuity constraint.

2.3. Decomposition of the conservative variables in a premixed flame brush

If the jumps in filtered density and momentum through the flame brush are discretized on few points, they can be represented with a single function $\bar{\alpha}$ that is unity in the burned gases and equal to zero in the unburned gases:

$$\bar{\rho} = \bar{\alpha}\bar{\rho}_\mathrm{b} + (1-\bar{\alpha})\bar{\rho}_\mathrm{u}, \tag{7}$$

$$\bar{\rho}\tilde{\mathbf{u}} = \bar{\alpha}\bar{\rho}_\mathrm{b}\tilde{\mathbf{u}}_\mathrm{b} + (1-\bar{\alpha})\bar{\rho}_\mathrm{u}\tilde{\mathbf{u}}_\mathrm{u}. \tag{8}$$

The Favre average in (8) is defined with respect to the density in the burned and unburned gases:

$$\bar{\rho}_\mathrm{b}\tilde{\mathbf{u}}_\mathrm{b} = \overline{\rho_\mathrm{b}\mathbf{u}_\mathrm{b}}, \quad \bar{\rho}_\mathrm{u}\tilde{\mathbf{u}}_\mathrm{u} = \overline{\rho_\mathrm{u}\mathbf{u}_\mathrm{u}}. \tag{9}$$

This decomposition of (7) and (8) can be derived rigorously, assuming that the instantaneous flame is infinitely thin. Then, the instantaneous density and momentum can be decomposed identically:

$$\rho = \rho_\mathrm{u} + \alpha[\rho], \tag{10}$$

$$\rho\mathbf{u} = \rho_\mathrm{u}\mathbf{u}_\mathrm{u} + \alpha[\rho\mathbf{u}]. \tag{11}$$

where α is a Heavyside function, and $[\rho]$ and $[\rho\mathbf{u}]$ denote the density and momentum jumps. Filtering both equations gives:

$$\bar{\rho} = \bar{\rho}_\mathrm{u} + \bar{\alpha}[\bar{\rho}], \tag{12}$$

$$\bar{\rho}\tilde{\mathbf{u}} = \bar{\rho}_\mathrm{u}\tilde{\mathbf{u}}_\mathrm{u} + \overline{\alpha[\rho\mathbf{u}]}. \tag{13}$$

Eq. (7) is equivalent to (12), but (8) is equivalent to (13) if $\overline{\alpha[\rho\mathbf{u}]}$ is assumed to be equal to $\bar{\alpha}[\bar{\rho}\tilde{\mathbf{u}}]$. The error resulting from this assumption is localized in the region where $\bar{\alpha}$ is non-constant, i.e., in a grid cell, and it de-

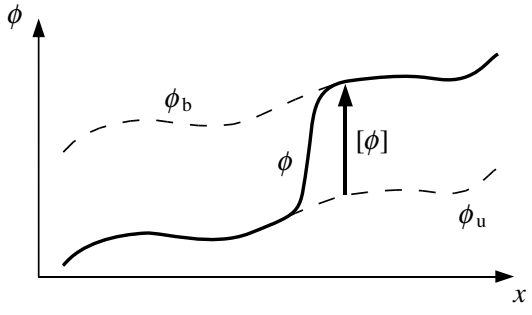

Fig. 1. The ghost-fluid method decomposition. ϕ_u and ϕ_b are the pre- and post-interface states, the unburned and burned gases in the case of premixed combustion, and $[\phi]$ is the jump.

pends on the fluctuations of the momentum jump $[\rho\mathbf{u}]$. Using the jump conditions derived in Section 2.6, this jump can be rewritten as $[\rho](\mathbf{u}_u + S_{L,u}\mathbf{N})$, where $S_{L,u}\mathbf{N}$ is the intrinsic flame speed. This implies that the error is proportional to the fluctuations of the speed in the unburned gases $\mathbf{u}_u$. In practical applications, the combustion takes place in the corrugated flamelet regime or in the thin reaction zones regime. In these regimes, the turbulent fluctuations are small compared to the jump created by thermal expansion in the reaction zone of the flame. The decomposition (8) is therefore a good approximation. Nevertheless, for very high Reynolds number flows where the flame cannot be considered as a jump compared to the turbulent structures or for flames with low heat release, the decomposition (8) may produce errors.

2.4. The continuity constraint

The continuity constraint (1) can be reformulated using (7) and (8). Further assuming that the continuity is satisfied in the burned and unburned gases leads to:

$$\frac{\partial\bar{\alpha}}{\partial t} + \frac{[\bar{\rho}\tilde{\mathbf{u}}]}{[\bar{\rho}]}\cdot\nabla\bar{\alpha} = 0, \tag{14}$$

where $[\bar{\rho}]$ and $[\bar{\rho}\tilde{\mathbf{u}}]$ denote the density and momentum jumps. The continuity constraint therefore leads to a propagation equation for the flame profile. If $\bar{\alpha}$ is only a function of the level set field G, then (14) is also a constraint on G:

$$\frac{\partial G}{\partial t} + \frac{[\bar{\rho}\tilde{\mathbf{u}}]}{[\bar{\rho}]}\cdot\nabla G = 0. \tag{15}$$

2.5. The coupled Poisson equation

The fractional-step algorithm presented in Section 2.1 is supposed to be satisfied for the burned, unburned, and global quantities through the flame brush. Then, if the pressure gradient is decomposed similar to the conservative variables:

$$\nabla\overline{P} = \bar{\alpha}\nabla\overline{P}_b + (1-\bar{\alpha})\nabla\overline{P}_u, \tag{16}$$

the pressure Laplacian of (6) becomes:

$$\nabla\cdot\nabla\overline{P} = \bar{\alpha}\nabla\cdot\nabla\overline{P}_b + (1-\bar{\alpha})\nabla\cdot\nabla\overline{P}_u + [\nabla\overline{P}]\cdot\nabla\bar{\alpha}. \tag{17}$$

The two first terms on the RHS of (17) are the pressure Laplacians in the burned and unburned gases multiplied by the profile function. The third term is the pressure gradient jump which is related to the momentum jump as shown in Section 2.6. The two Laplacians can be expressed as functions of the density variations and of the predicted velocity divergence on both sides of the flame. This leads to the coupled Poisson equation:

$$\nabla\cdot\nabla\overline{P} = [\nabla\overline{P}]\cdot\nabla\bar{\alpha} + \frac{1}{\Delta t}\left(\bar{\alpha}\frac{\partial\bar{\rho}_b}{\partial t} + (1-\bar{\alpha})\frac{\partial\bar{\rho}_u}{\partial t} + \bar{\alpha}\nabla\cdot\bar{\rho}_b\tilde{\mathbf{u}}_b^{\star} + (1-\bar{\alpha})\nabla\cdot\bar{\rho}_u\tilde{\mathbf{u}}_u^{\star}\right). \tag{18}$$

Then, the pressure gradients in the unburned and burned gases are found by using the expressions:

$$\nabla\overline{P}_u = \nabla\overline{P} - \bar{\alpha}[\nabla\overline{P}], \quad \nabla\overline{P}_b = \nabla\overline{P} + (1-\bar{\alpha})[\nabla\overline{P}]. \tag{19}$$

It should be noted that $\nabla\overline{P}_u$ and $\nabla\overline{P}_b$ are not real pressure gradients but simply momentum corrections to impose the divergence and the jump constraints.

2.6. Jump conditions

The density jump $[\bar{\rho}]$ is given by the thermo-chemistry in the flame, and it is an input of the computation. The momentum jump is obtained from the continuity equation expressed in a Galilean frame that is moving at a speed $\mathbf{U}_S$ in the reference frame. The flame is then steady in this frame, and the continuity equation becomes:

$$\nabla \cdot (\bar{\rho}(\tilde{\mathbf{u}} - \mathbf{U}_S)) = 0. \tag{20}$$

Integrating this equation in the flame brush leads to:

$$[\bar{\rho}\tilde{\mathbf{u}}] = [\bar{\rho}]\mathbf{U}_S. \tag{21}$$

The frame speed $\mathbf{U}_S$ can be expressed as the sum of a flow speed and an intrinsic flame speed. Taking these values in the unburned gases gives:

$$[\bar{\rho}\tilde{\mathbf{u}}] = [\bar{\rho}](\tilde{\mathbf{u}}_u + S_{T,u}\mathbf{N}), \tag{22}$$

where $\mathbf{N}$ is the flame brush normal:

$$\mathbf{N} = -\frac{\nabla G}{\|\nabla G\|}. \tag{23}$$

The level set propagation equation given by (15) can therefore be rewritten in the usual form:

$$\frac{\partial G}{\partial t} + (\tilde{\mathbf{u}}_u + S_{T,u}\mathbf{N}) \cdot \nabla G = 0. \tag{24}$$

Finally, the jump of the gradient of the dynamic pressure $[\nabla \overline{P}]$ is obtained taking the difference of the pressure correction steps in the burned and unburned gases:

$$[\nabla \overline{P}] = \frac{1}{\Delta t}([\bar{\rho}\tilde{\mathbf{u}}^{\star}] - [\bar{\rho}\tilde{\mathbf{u}}^{n+1}]). \tag{25}$$

2.7. The combustion model

To determine the burning velocity in the unburned gases $S_{T,u}$, the LES model developed by Pitsch [7] is used. This model is an extension of the G-equation model originally derived for the Reynolds-averaged Navier–Stokes (RANS) formalism [3,4]. The burning velocity $S_{T,u}$ is given by the relation [5]:

$$\frac{S_{T,u} - S_{L,u}}{S_{L,u}} = -\frac{b_3^2 C_s}{2b_1 \mathrm{Sc}_{t,G}} \frac{\Delta}{l_F} + \sqrt{\left(\frac{b_3^2 C_s}{2b_1 \mathrm{Sc}_{t,G}} \frac{\Delta}{l_F}\right)^2 + \frac{b_3^2 D_{t,G}}{S_{L,u} l_F}}, \tag{26}$$

where $S_{L,u}$ is the laminar burning velocity, Δ is the filter width, l_F is the laminar flame thickness, C_s is the Smagorinsky constant, $\mathrm{Sc}_{t,G} = 0.5$ is a turbulent Schmidt number, and $b_1 = 2.0$ and $b_3 = 1.0$ are two model constants. The turbulent diffusivity $D_{t,G}$ is computed using a Smagorinsky-type model:

$$D_{t,G} = \frac{C_s \Delta u'_\Delta}{\mathrm{Sc}_{t,G}}. \tag{27}$$

where u'_Δ is the intensity of the sub-filter velocity fluctuations.

2.8. The full algorithm

The full algorithm consists of the following steps:

Step 1: Advance the level set equation from $G^{n+1/2}$ to $G^{n+3/2}$
The propagation equation given by (24) is advanced with estimates of $\tilde{\mathbf{u}}_u^{n+1}$ and $S_{T,u}^{n+1}$. These estimates can be given by a first-order Adams–Bashforth scheme or simply by taking the values of the previous time step $\tilde{\mathbf{u}}_u^n$ and $S_{T,u}^n$. The second method is used in the presented test cases and gives satisfactory results. The time integration is done using a 3-step back and forth error correction (BFEC) method [8], and the spatial discretization is done using a first-order upwind scheme. The combination of these two integration techniques leads to a low-dispersion and low-dissipation scheme that is second-order in space and time [8]. Then, to keep the level set field G equal to a distance function, a fast-marching reinitialization method [9] is used.

Step 2: Compute the flame brush profile $\bar{\alpha}^{n+3/2}$ and the density field $\bar{\rho}^{n+3/2}$
These two quantities are computed using a user-defined profile for $\bar{\alpha}^{n+3/2}$, which is a function of the distance to the flame front. If the instantaneous flame is largely under-resolved on the mesh, which is the case in most practical applications, then the thickness of the flame profile $\bar{\alpha}^{n+3/2}$ has to be of the order of the grid spacing. For the turbulent cases of Section 3, the profile was chosen to be $(1+\sin(\pi\times G/\delta))/2$ in the flame front, where δ was taken approximately equal to six times the grid spacing. This leads to a thermal thickness, i.e., the thickness of the temperature jump based on the maximum gradient, of approximately two cells. Then, the density is computed according to (7), where the density in the burned and the unburned gases is taken constant.

Step 3: Advance the momentum in the unburned and burned gases $\bar{\rho}_u\tilde{\mathbf{u}}_u^\star$ and $\bar{\rho}_b\tilde{\mathbf{u}}_b^\star$
The momentum in the unburned and in the burned gases is advanced independently following (4) and using an implicit Gauss-Seidel method with relaxation. The spatial scheme is second-order central and conserves the kinetic energy [10].

Step 4: Compute the pressure gradient jump $[\nabla\overline{P}]$
This jump is computed according to (25), in which the momentum jump at t^{n+1} is evaluated using (22).

Step 5: Solve the Poisson equation
This constant-coefficient Poisson equation (18) is solved using the algebraic multi-grid solver of the Hypre library from Lawrence Livermore National Laboratory [11].

Step 6: Correct the unburned and burned momentum
The pressure gradients in the unburned and burned gases are computed using (19) and are then used to correct the momentum in the unburned and burned gases.

It may be noted that compared to a classical low-Mach solver with a combustion model based on a level set transport, this algorithm only requires the solution of an additional set of momentum equations. Moreover, since no jumps appear in the spatial derivatives, this algorithm usually converges faster than a classical solver and it does not require any sub-stepping which would dramatically reduce the efficiency.

3. Results

In this section, the proposed method is verified by computing 2D flame–vortex interactions. Then, the method is applied to the LES computation of a turbulent flame anchored by a triangular flame holder. Finally, LES computations of a reacting industrial lean-premixed swirl-burner are presented and discussed.

3.1. Flame–vortex interactions

The proposed method is verified by computing 2D flame–vortex interactions. This unsteady laminar test case has been studied experimentally [12], and it has been extensively used to build DNS databases and combustion regime diagrams [13], and to validate combustion models [1]. Recently, Lessani and Papalexandris [14] have used this test to verify a low-Mach fractional-step method.

The flame–vortex computations performed in this study consist of a steady laminar premixed flame interacting with a vortex dipole convected at the laminar burning speed. The parameters used in this study are the same as in Ref. [14] (Le = 1, $r/\delta = 5.5$, $u'/S_L = 10.6$), and these parameters are close to one case of the database of Poinsot et al. [13] (Le = 1.2, $r/\delta = 5$, $u'/S_L = 12$). The flame profile $\bar{\alpha}$ has been extracted from the 1D computations of Ref. [14]. The initial conditions are given in Fig. 2a. The distances are non-dimensionalized by the flame thickness. The inlet is located at $Y = 0$ and the inlet velocity is set equal to the burning velocity S_L. Before the interaction with the vortex dipole, the flame is steady and located at $Y = 100$. When the vortices arrive in the vicinity of the flame, their vorticity decreases rapidly as they wrinkle the flame front. Between the vortices, the flow speed increases, whereas on the sides of the dipole the flow speed decreases. It leads to the formation of an unburned gas pocket as shown in Fig. 2b. The form of the flame on this figure is very close to the results of Ref. [13].

For a verification of the proposed method, a mesh refinement study is performed. Three Cartesian meshes of dimensions 64×256, 128×256 and 256×512 are used. The discretization of the flame profile for the

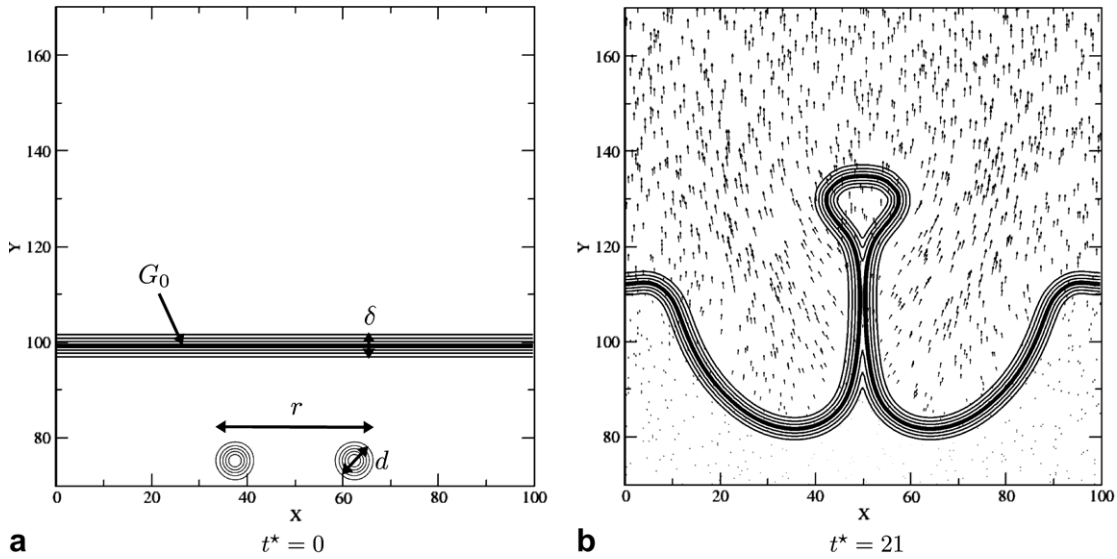

Fig. 2. Flame–vortex interactions. G_0-level set (bold), density contours (thin lines, around G_0) and velocity vectors (arrows) for the finest mesh (256×512). The time is non-dimensionalized by the chemical time scale δ/S_L. (a) $t^\star = 0$; (b) $t^\star = 21$.

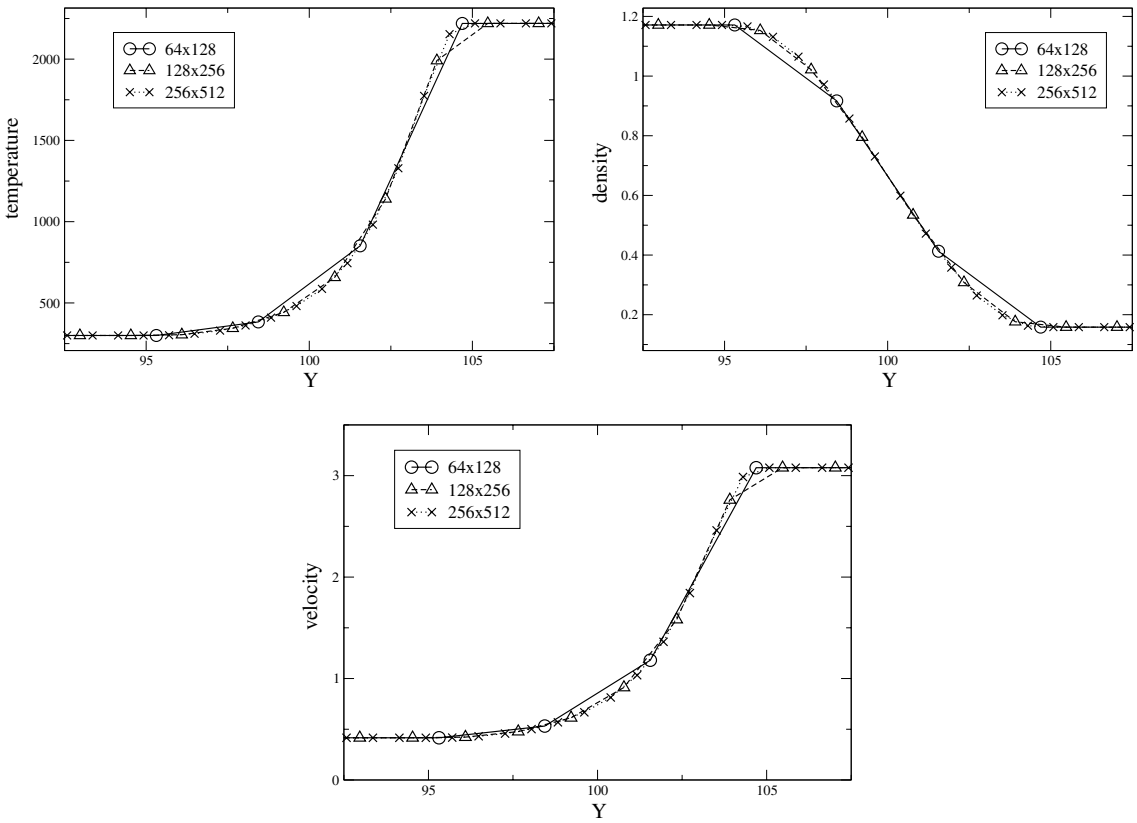

Fig. 3. Flame–vortex interactions. Discrete flame profiles for the different mesh resolutions.

different mesh resolutions is shown in Fig. 3. It may be noted that on the coarse grid the flame is resolved on only three points. Snapshots of the G_0-level set are presented in Fig. 4. The results obtained with the three different resolutions are in very good agreement, and they show the same behavior as those obtained by

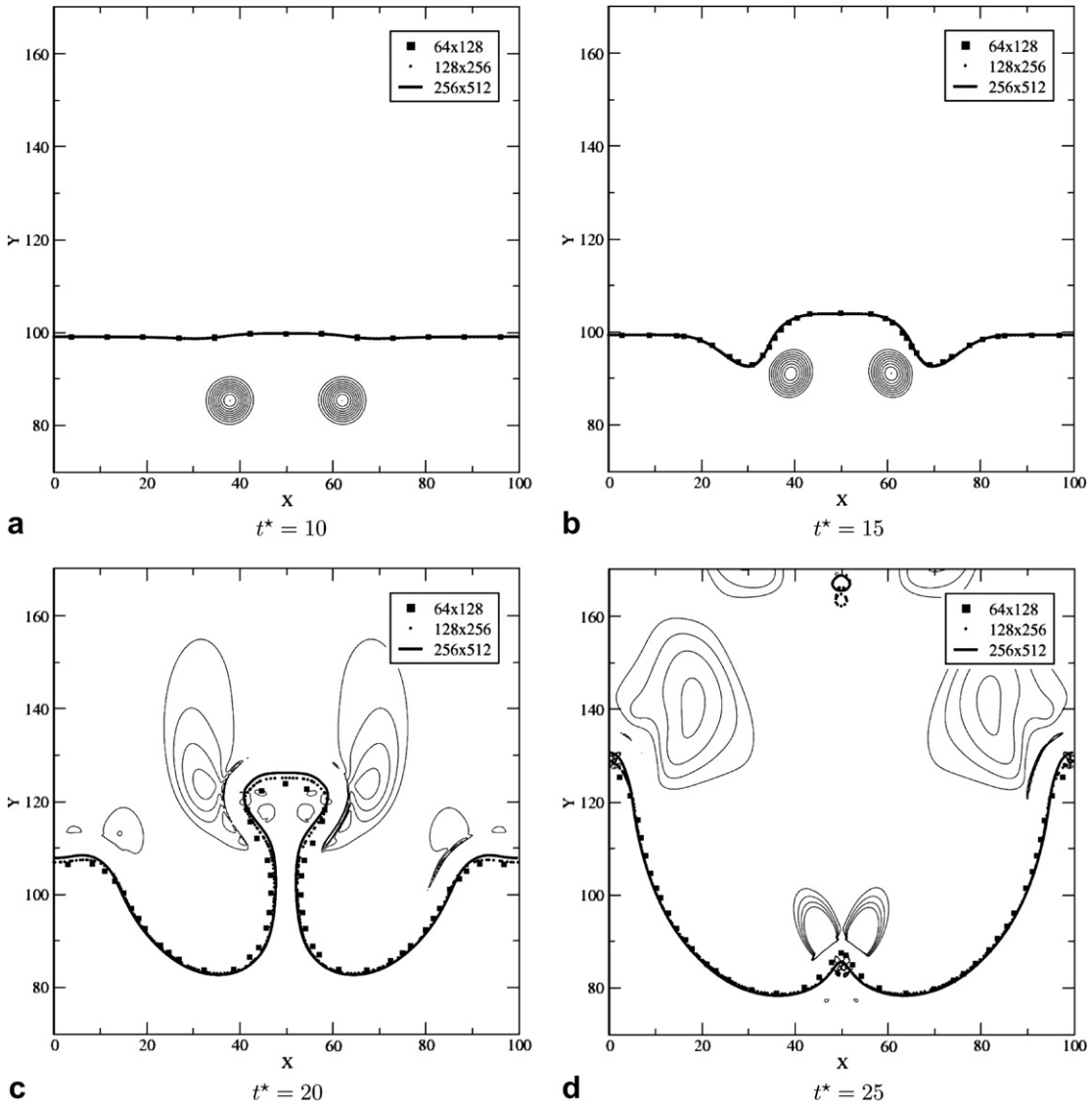

Fig. 4. Flame–vortex interactions. G_0 level set for 3 different meshes and Q criterion [17] contours for the finer mesh.

Poinsot et al. [13]. However, the results are quite different from those of Lessani and Papalexandris [14], in which no pocket of unburned gas is formed. These differences can be explained by the fact that the formation of this pocket is very sensitive to the numerical dissipation and to the actual burning velocity of the flame. In Ref. [14], a predictor-corrector technique and second-order centered schemes are used as in the proposed method. Nevertheless, the time integration does not ensure the kinetic-energy conservation and the flame propagation relies on a reaction-diffusion balance, which requires a fine resolution to be accurate. The kinetic-energy conservation and the flame propagation are the main impetus for using a level set formalism coupled to kinetic-energy conserving schemes in the present method.

3.2. Triangular flame-holder

3.2.1. Description

This configuration consists of a turbulent premixed flame anchored to a triangular flame-holder. It has been studied experimentally [15,16] with the objective of providing data for the validation of RANS and LES

Table 1
Triangular flame-holder parameters

Re	u_{in}	ϕ	S_L	δ	ρ_u	ρ_b	ρ_u/ρ_b
33,000	20 m/s	1	0.41 m/s	0.37 mm	1.19 kg/m^3	0.14 kg/m^3	8.5

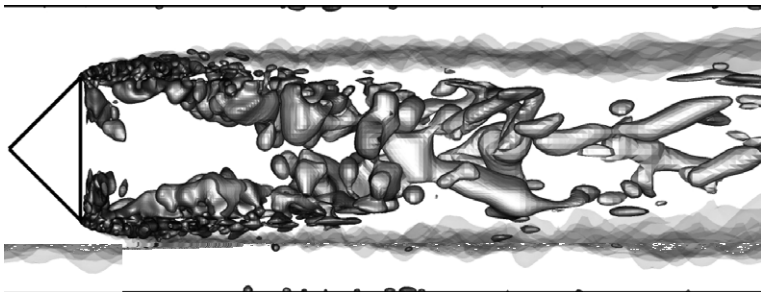

Fig. 5. Triangular flame-holder. Flame (transparent) and Q criterion [17] contours.

combustion models. This burner is operated at atmospheric conditions with a stoichiometric propane–air mixture. The inlet speed u_{in} and the main flame characteristics are given in Table 1. A 3D computation of this configuration has been performed with an unstructured mesh of approximatively 2 million hexahedral cells. The flame profile $\bar{\alpha}$ has been chosen to give a constant thermal thickness approximately equal to twice the filter width near the flame-holder. A snapshot of the computed flame and of the coherent structures of the flow is presented in Fig. 5. The Q criterion [17], which is the second invariant of the deformation tensor, is used to visualize the coherent structures. It compares the magnitude of the rotation and shear rates. Most of the vortices are created in the shear zone between the flame-holder recirculation and the burned gases accelerated by the thermal expansion. These vortices, which are originally transverse, are elongated by the burned gases and become streamwise in the tail of the recirculation zone.

3.2.2. Progress-variable statistics

The values of the mean progress-variable $\bar{c}$ given by the 3D LES computation and extracted from OH-LIF images are compared in Fig. 6. The contours are in good agreement, demonstrating that the dynamics of the flame are captured accurately by the LES computation. The four dashed lines in Fig. 6 represent the locations chosen to compare the mean and RMS progress-variable profiles. The results of these are given in Fig. 7. The RMS profiles are reconstructed from the mean progress variable assuming that the flame is infinitely thin [18]:

$$c_{rms} = \sqrt{\bar{c}(1-\bar{c})}. \tag{28}$$

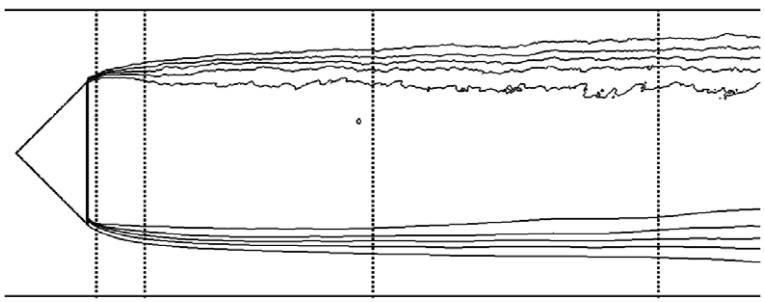

Fig. 6. Triangular flame-holder. Experimental (top) and LES (bottom) mean progress-variable contours.

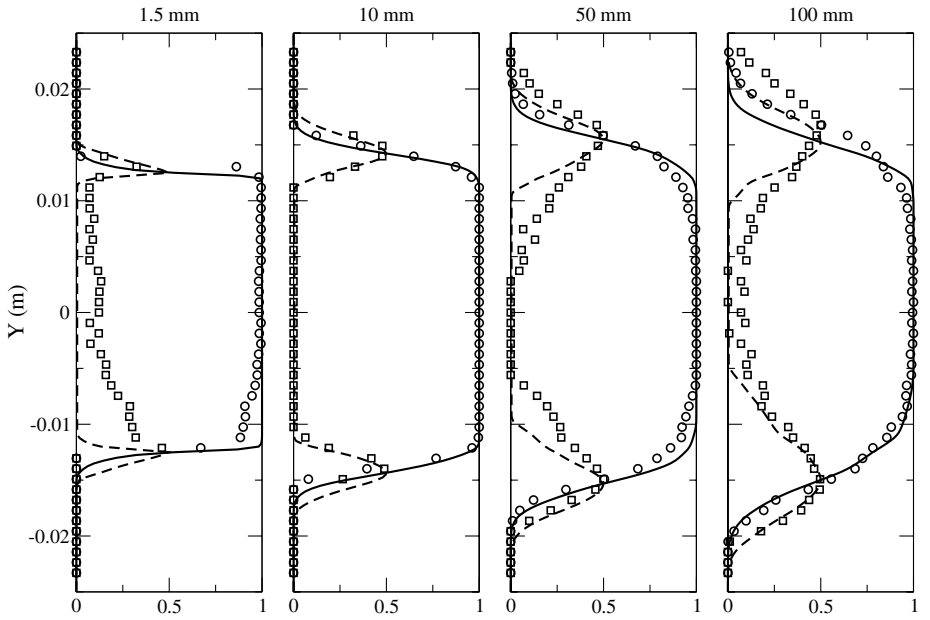

Fig. 7. Triangular flame-holder. Mean and RMS progress-variable profiles. ○ and □: $\bar{c}$ and c_{rms} from experiments, — and ----: $\bar{c}$ and c_{rms} from LES.

The mean and RMS progress-variable profiles, shown in Fig. 7, are in very good agreement with experimental data. The discrepancies in the RMS profiles far from the flame-holder are probably due to the fact that the filtered flame thickness is taken constant in the entire domain.

3.3. Industrial lean-premixed swirl-burner

3.3.1. Description

In this section, the proposed method is applied in a simulation of a complex swirl-burner shown in Fig. 8. It features a plenum, a swirl-injector and a combustion chamber. A lean premixed mixture of methane and air is

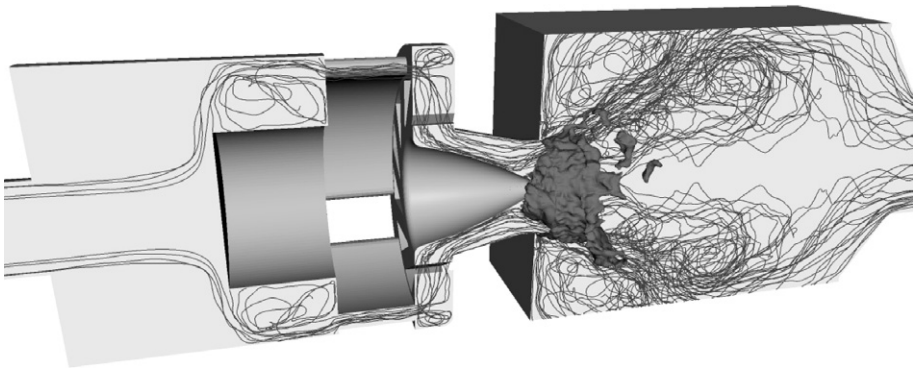

Fig. 8. Swirl-burner. Instantaneous flame and azimuthally-projected stream-lines.

Table 2
Swirl-burner parameters

Re	u_{in}	ϕ	S_{L}	δ	ρ_{u}	ρ_{b}	$\rho_{\mathrm{u}}/\rho_{\mathrm{b}}$
45,000	24 m/s	0.75	0.23 m/s	0.6 mm	1.14 kg/m^3	0.18 kg/m^3	6.3

injected at atmospheric pressure in the plenum, and the turbulent flame is anchored at the outlet of the swirler. The swirl plays an important role in the stabilization of the lean premixed flame. The main parameters of the burner are given in Table 2. Velocity LDV measurements [19] are available for several locations in the combustion chamber. This burner has been computed by [19] using the thickened-flame model (TFLES) [1], and their results are in good agreement with experimental data.

Two different unstructured meshes have been used to perform the LES computations. The first is based mostly on tetrahedral elements and is the same as in [19]. The second is based mostly on hexahedral elements. Both meshes consist of approximately three million control volumes. Given these meshes, the computed turbulent flames can be located in the LES combustion diagram (Fig. 9) proposed by [7]. These flames are at the interface between the thin reaction zones regime and the broken reaction zones regime. The combustion model described in Section 2.7 is actually valid only for the corrugated and the thin reaction zones regimes. The flame profile $\bar{\alpha}$ has been defined to give a thermal thickness approximately equal to twice the filter width.

The flame structure and the coherent structures of the flow are presented in Fig. 10. The vortices are formed in two main regions. The first region is the sudden enlargement on the exterior of the swirler, and the second region is the head of the injector, where the separation of the flow occurs. While the exterior vortices are of

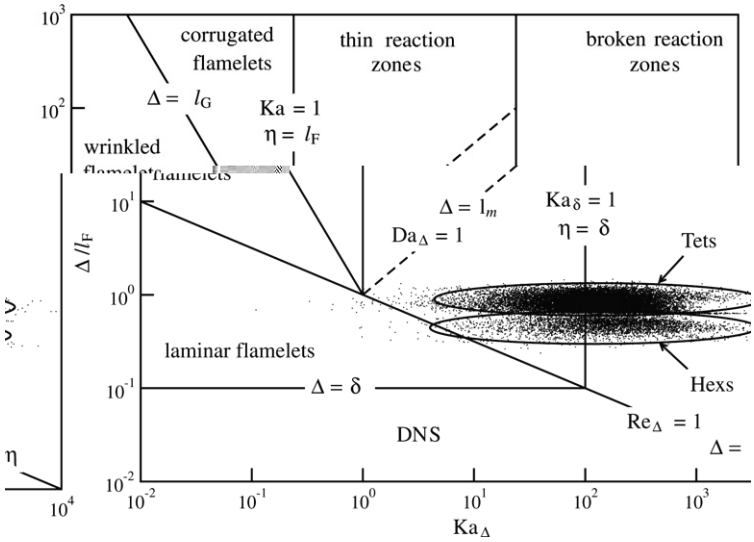

Fig. 9. Swirl-burner. Location of the computations in the LES regime diagram.

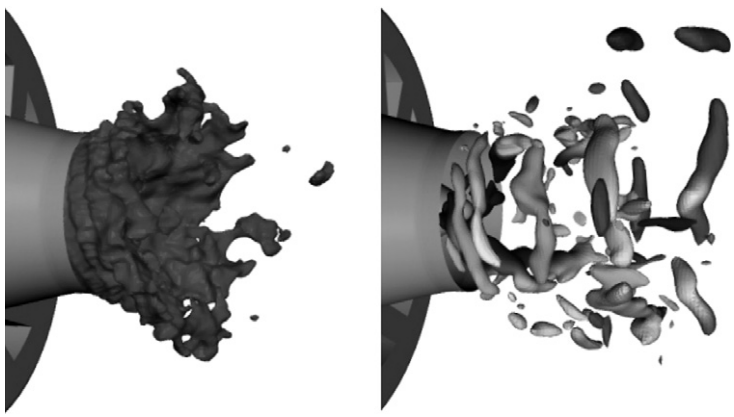

Fig. 10. Swirl-burner. Flame (left) and coherent structures in the flame colored by the distance to the axis (right).

small intensity, the vortices in the core region strongly affect the flame brush. The interior vortices are of the same nature as the precessing vortex core (PVC) described by [19] for the non-reactive flow.

3.3.2. Velocity statistics

The mean and RMS velocities from the LES computations are compared to the experimental data in Figs. 11–16. The comparisons are performed for five 1D profiles at different distances from the chamber head. Both

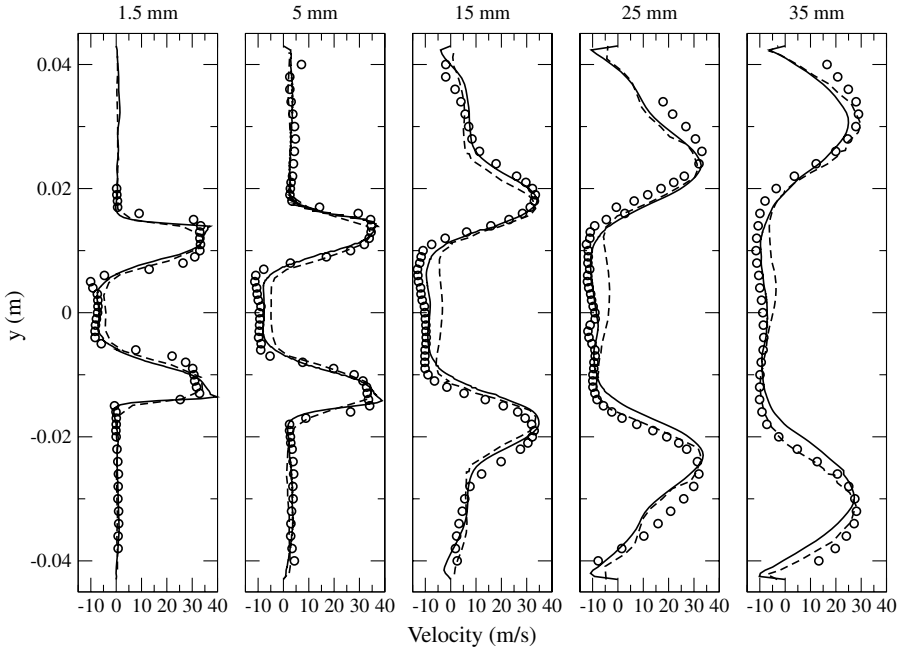

Fig. 11. Swirl-burner. Mean axial velocity profiles. ○, experiments; —, LES on the hexahedral mesh; ----, LES on the tetrahedral mesh.

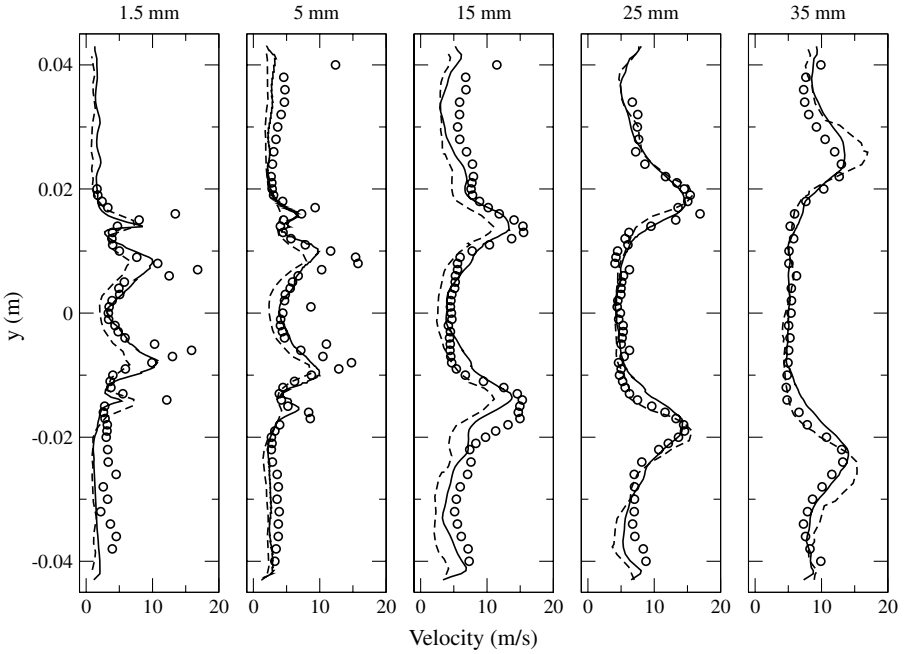

Fig. 12. Swirl-burner. Axial velocity RMS profiles. ○, experiments; —, LES on the hexahedral mesh; ----, LES on the tetrahedral mesh.

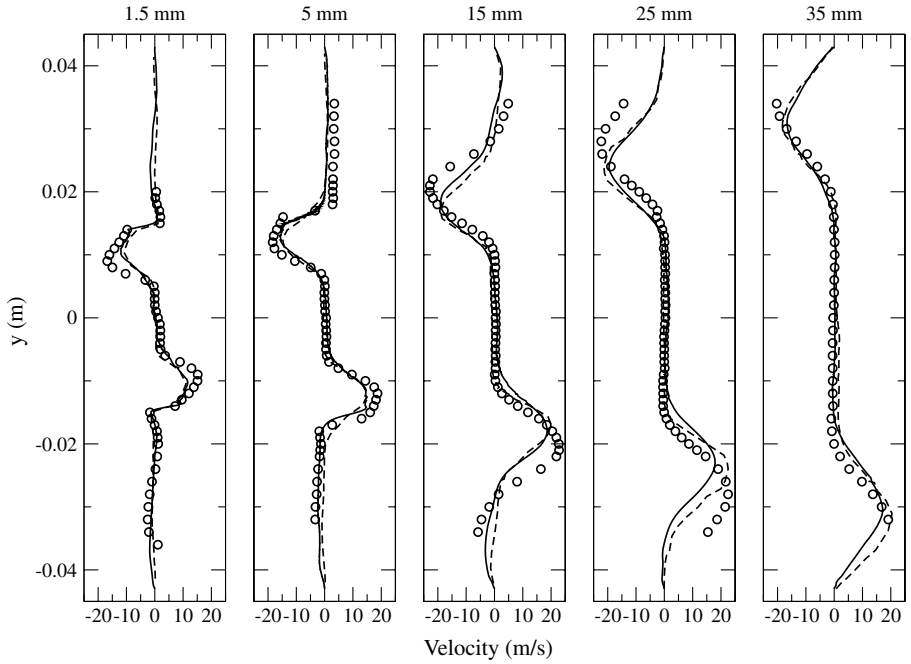

Fig. 13. Swirl-burner. Mean radial velocity profiles. ○, experiments; —, LES on the hexahedral mesh; ----, LES on the tetrahedral mesh.

mean and RMS profiles are in a very good agreement, especially in the near field of the injector. The 1.5 mm RMS profiles in Fig. 16 clearly show the velocity fluctuations due to the exterior and interior vortices. The exterior vortices are well captured on both meshes by the present method, whereas they do not seem to be captured in [19]. This difference may be due to the thickened-flame combustion model or to the spatial differencing used in [19].

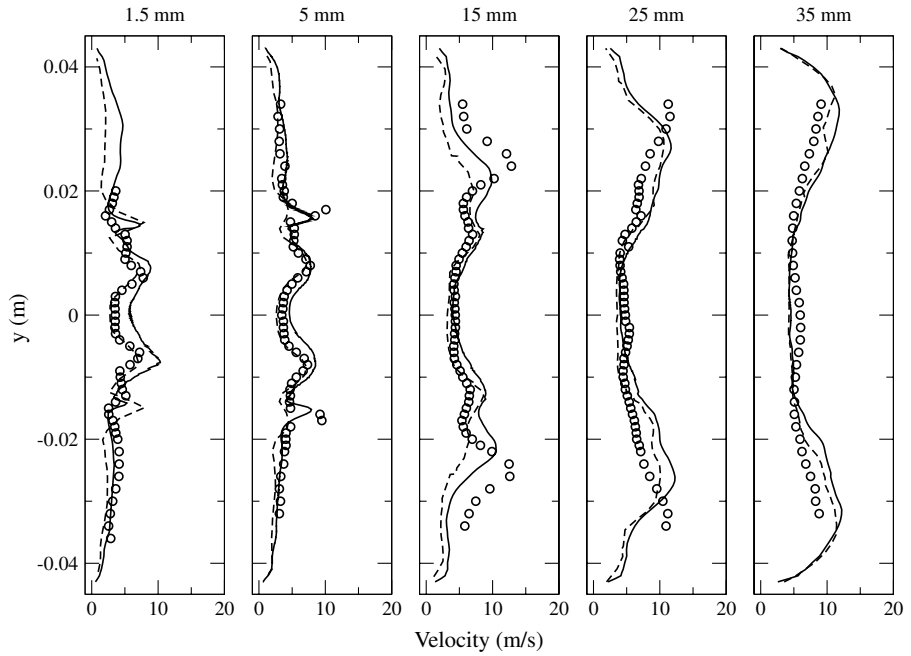

Fig. 14. Swirl-burner. Radial velocity RMS profiles. ○, experiments; —, LES on the hexahedral mesh; ----, LES on the tetrahedral mesh.

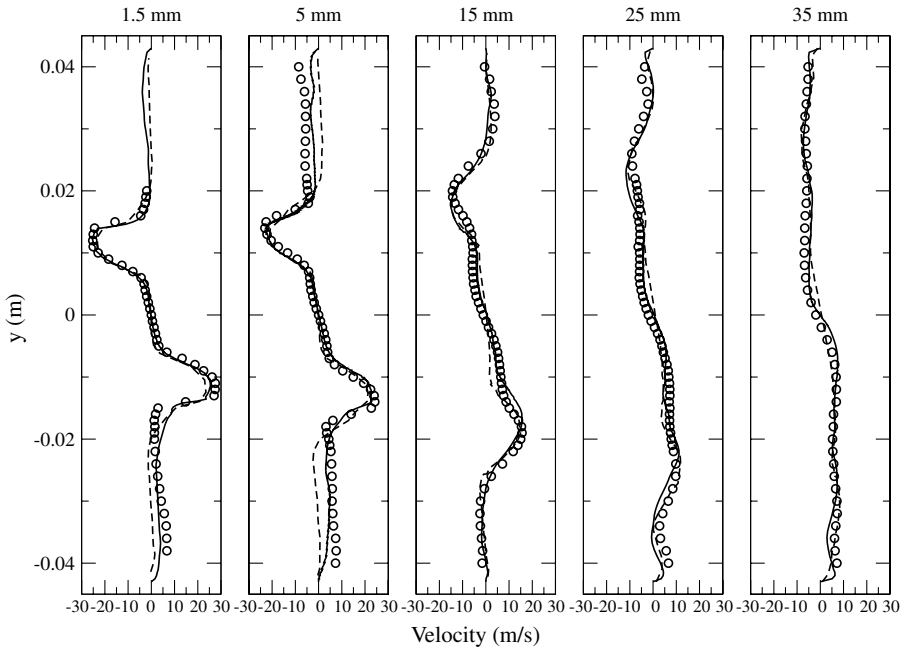

Fig. 15. Swirl-burner. Mean tangential velocity profiles. ○, experiments; —, LES on the hexahedral mesh; ----, LES on the tetrahedral mesh.

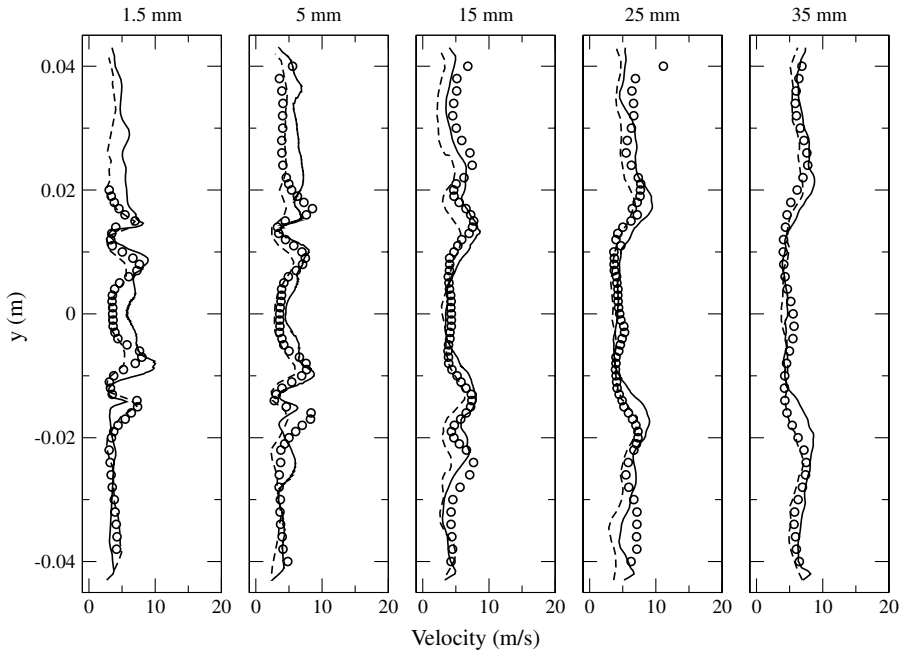

Fig. 16. Swirl-burner. Tangential velocity RMS profiles. ○, experiments; —, LES on the hexahedral mesh; ----, LES on the tetrahedral mesh.

4. Conclusions

A new ghost-fluid method for premixed flames of finite thickness has been developed. This method provides a robust and accurate coupling of the *G*-equation model with a low-Mach Navier–Stokes solver while allowing

for the use of kinetic-energy conserving schemes. The combination of these state-of-the-art algorithms results in a very accurate description of the flame transport and ensures very low numerical dissipation. The proposed method has first been verified using the basic test case of laminar flame–vortex interactions. The results demonstrate the high accuracy of the method even on coarse meshes. Furthermore, the method has been applied in the LES computation of a turbulent flame anchored by a triangular flame-holder. Computed mean and RMS progress-variable profiles are compared to the experimental data showing good agreement. Finally, the method has been used to compute the combustion process in a complex swirl-burner. The dynamic behavior of the device is discussed and mean and RMS velocity profiles are compared with experimental measurements. The very good agreement obtained for this complex geometry assesses the high fidelity of the method.

Acknowledgments

The authors gratefully acknowledge funding by SAFRAN Group and the Air Force Office of Scientific Research. We thank Prof. Veynante for his assistance in providing data from the triangular flame-holder experiment.

References

[1] O. Colin, F. Ducros, D. Veynante, T. Poinsot, A thickened flame model for large-eddy simulations of turbulent premixed combustion, Phys. Fluids. 12 (7) (2000) 1843–1863.
[2] M. Boger, D. Veynante, H. Boughanem, A. Trouve, Direct numerical simulation analysis of flame surface density concept for large-eddy simulation of turbulent premixed combustion, in: Proceedings of the Twenty-seventh Symposium (Int.) on Combustion, The Combustion Institute, Pittsburgh, Boulder, 1998, pp. 917–927.
[3] F. Williams, Combustion Theory, Benjamin Cummings, Menlo Park, CA, 1985.
[4] N. Peters, Turbulent Combustion, Cambridge University Press, Cambridge, UK, 2000.
[5] H. Pitsch, L. Duchamp de Lageneste, Large-eddy simulation of premixed turbulent combustion using a level set approach, Proc. Combust. Inst. 29 (2002) 2001–2008.
[6] R. Fedkiw, T. Aslam, B. Merriman, S. Osher, A non-oscillatory Eulerian approach to interfaces in multimaterial flows (the ghost-fluid method), J. Comput. Phys. 152 (1998) 457–492.
[7] H. Pitsch, A consistent level set formulation for large-eddy simulation of premixed turbulent combustion, Combust. Flame 143 (2005) 587–598.
[8] T.F. Dupont, Y. Liu, Back and forth error compensation and correction methods for removing errors induced by uneven gradients of the level set function, J. Comput. Phys. 190 (1) (2003) 311–324.
[9] J.A. Sethian, A fast marching level set method for monotonically advancing fronts, Proc. Natl. Acad. Sci. 93 (1996) 1591–1595.
[10] K. Mahesh, G. Constantinescu, P. Moin, A numerical method for large-eddy simulation in complex geometries, J. Comput. Phys. 197 (1) (2004) 215–240.
[11] R. Falgout, U. Yang, Hypre: a library of high-performance preconditioners, Lecture Notes in Computer Science 2331 (2002) 632–641.
[12] C.J. Mueller, J.F. Driscoll, D.L. Reuss, M.C. Drake, M.E. Rosalik, Vorticity generation and attenuation as vortices convect through a premixed flame, Combust. Flame 112 (3) (1998) 342–358.
[13] T. Poinsot, D. Veynante, S. Candel, Quenching processes and premixed turbulent combustion diagrams, J. Fluid Mech. 228 (1991) 561–606.
[14] B. Lessani, M.V. Papalexandris, Time-accurate calculation of variable density flows with strong temperature gradients and combustion, J. Comput. Phys. 212 (2006) 218–246.
[15] C. Nottin, R. Knikker, M. Boger, D. Veynante, Large eddy simulations of an acoustically excited turbulent premixed flame, in: Proceedings of the Twenty-eighth Symposium (Int.) on Combustion, 2000, pp. 67–73.
[16] R. Knikker, D. Veynante, C. Meneveau, A priori testing of a similarity model for large-eddy simulations of turbulent premixed combustion, in: Proceedings of the Twenty-ninth Symposium (Int.) on Combustion, vol. 2, 2002, pp. 2105–2111.
[17] Y. Dubief, F. Delcayre, On coherent-vortex identification in turbulence, J. Turbulence 1 (2000) 1–22.
[18] T. Poinsot, D. Veynante, Theoretical and Numerical Combustion, R.T. Edwards, 2001.
[19] S. Roux, G. Lartigue, T. Poinsot, U. Meier, C. Berat, Studies of mean and unsteady flow in a swirled combustor using experiments, acoustic analysis, and large-eddy simulations, Combust. Flame 141 (1–2) (2005) 40–54.